Mutual Neutralization of O^- with O^+ and N^+ at Subthermal Collision Energies

N. de Ruette,[1] A. Dochain,[2] T. Launoy,[3] R. F. Nascimento,[4,1] M. Kaminska,[1,5] M. H. Stockett,[1] N. Vaeck,[3] H. T. Schmidt,[1] H. Cederquist,[1] and X. Urbain[2]

[1]*Department of Physics, Stockholm University, Stockholm, SE-106 91, Sweden*

[2]*Institute of Condensed Matter and Nanosciences, Université catholique de Louvain, B-1348 Louvain-la-Neuve, Belgium*

[3]*Laboratoire de Chimie Quantique et Photophysique, Université Libre de Bruxelles, B-1050 Brussels, Belgium*

[4]*Centro Federal de Educação Tecnológica Celso Suckow da Fonseca, Petrópolis, 25620-003 RJ, Brazil*

[5]*Institute of Physics, Jan Kochanowski University, 25-369 Kielce, Poland*

(Received 24 April 2018; published 22 August 2018)

We have measured total absolute cross sections for the mutual neutralization (MN) of O^- with O^+ and N^+. A fine resolution (of about 50 meV) in the kinetic energy spectra of the product neutral atoms allows unique identification of the atomic states participating in the mutual neutralization process. Cross sections and branching ratios have also been calculated down to 1 meV center-of-mass collision energy for these two systems, with a multichannel Landau-Zener model and an asymptotic method for the ionic-covalent coupling matrix elements. The importance of two-electron processes in one-electron transfer is demonstrated by the dominant contribution of a core-excited configuration of the nitrogen atom in $N^+ + O^-$ collisions. This effect is partially accounted for by introducing configuration mixing in the evaluation of coupling matrix elements.

DOI: 10.1103/PhysRevLett.121.083401

Anions play crucial roles in a range of astrophysical environments and planetary atmospheres [1–7]. Reactions with atomic and molecular anions have been included in interstellar chemistry models [8,9] for decades, but it was not until 2006 that the first negative molecular ion, C_6H^-, was observed in molecular clouds [10]. Since then, C_4H^- [11], C_8H^- [12], C_3N^- [13], C_5N^- [14], and most recently CN^- [15], have also been detected. Anions often have loosely bound outer electrons and large reactivities, and may thus influence the charge balance in plasma even at low concentrations. Therefore, atomic anion formation processes such as dissociative ($AB + e^- \rightarrow A^- + B$) and radiative ($A + e^- \rightarrow A^- + h\nu$) attachment are of large interest for, e.g., astrophysical modeling [3,16]. Likewise, atomic anion *destruction* processes such as photodetachment ($A^- + h\nu \rightarrow A + e^-$), associative detachment ($A^- + B \rightarrow AB + e^-$), associative ionization (AI) ($A^- + B^+ \rightarrow AB^+ + e^-$), and mutual neutralization (MN)

$$A^- + B^+ \rightarrow A + B \tag{1}$$

are important in such contexts. The corresponding absolute cross sections and rate coefficients are thus key to determine charge balances, electron concentrations, and abundances of different species (in the forms of neutrals and ions) in cold molecular clouds and in other astrophysical environments [3,16–24]. Likewise, in Earth's ionosphere, an accurate estimation of the contribution of $O^- + O^+ \rightarrow O^* + O$ MN reactions to the ultraviolet equatorial nightglow is crucial to determine the nighttime ionospheric electron density [25–27]. MN reactions lead to the production of excited atomic oxygen atoms O^*, which then emit 135.6 nm photons via the radiative cascade $O(^5P) \rightarrow O(^5S) \rightarrow O(^3P)$.

Earlier experiments on mutual neutralization have mostly been performed at collision energies above some tenths of an eV. This energy range is not the most relevant for many astrophysical applications, and different final quantum states were not resolved in these earlier studies [28,29]. With the present experimental technique, two copropagating atomic ion beams are merged such that the angles between individual anion and cation trajectories are typically smaller than 1.5 mrad in the interaction region [30]. We are thus able to present the first subthermal studies of quantum-state resolved MN processes. We report results for the $O^- + O^+$ and $O^- + N^+$ MN reactions for center-of-mass collision energies between 5 meV and 2 eV. The mutual neutralization experiments were performed at the Université Catholique de Louvain. Studies of AI processes were previously performed with the same apparatus [31], and the corresponding results may be used to put the MN reaction cross sections on an absolute scale.

The negative ion beam O^- is produced by a Cs-ion sputter source from a Fe_2O_3 cathode. A Wien filter is used to select the ion mass. An electron cyclotron resonance (ECR) ion source followed by a bending magnet is used to form the O^+ and the N^+ beams. After the beams are shaped with ion optics and collimators [31], they are merged in a 6.8 ± 0.2 cm long interaction cell. The voltage on this cell can be fine-tuned in order to adjust the center-of-mass collision energy down to the meV range, where the lower limit is set by the angular spread within each of the ion

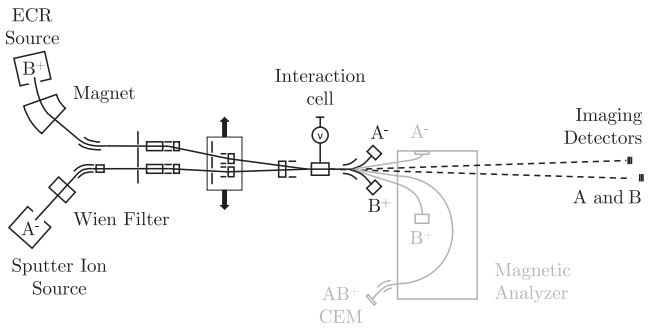

FIG. 1. Experimental apparatus (not to scale). The gray elements are used for associative ionization measurements.

beams and any (small) misalignment between them. The beams are demerged before leaving the ultrahigh vacuum section of the apparatus. A set of deflector plates after the interaction region is used to separate the ionic parent beams from the neutral products and to send the A^- and B^+ ion beams into separate Faraday cups, as shown in Fig. 1 (in black for MN and in gray for AI measurements). For the AI measurements, the product molecular ions AB^+ are deflected by a 180° magnet followed by a 30° deflector—to filter out scattered ions—and are sent into a single counting mode channel electron multiplier (CEM), as shown in gray in Fig. 1.

To detect the neutral products of mutual neutralization, we use a three-dimensional imaging detection system. It consists of two position sensitive detectors, each composed of a stack of three microchannel plates (MCPs) and a resistive anode. They are separated in the beam-propagation direction by 10 cm to reduce the dead zone between them. The kinetic energy release (KER) is determined from coincidence measurements of the positions and the differences in time of arrival of two neutrals (A and B) hitting separate detectors in a single MN event. The distortion on the positions caused by a nonlinear spatial response of the detectors is corrected for, and the background due to false coincidences is subtracted. The spectra are then corrected for the KER-dependent angular acceptance [32].

In contrast to earlier studies of MN [33], the use of two separate detectors allows for the simultaneous detection of the two products, and the long drift distance of 3.25 m from the interaction cell to the imaging detectors allows us to minimize the misalignment of the two beams. This is done by optimizing the MN coincidence rate relying on the (expected) $1/E_{\mathrm{CM}}$ energy dependence of the cross section and the fact that the angular dispersion of the beams is the main limiting factor for the resolution in the definition of the center-of-mass collision energy, E_{CM} [34]. Considering a collision between an anion of mass m_A and kinetic energy E_A, and a cation of mass m_B and kinetic energy E_B (E_A and E_B are the ion-beam energies in the laboratory system), we get

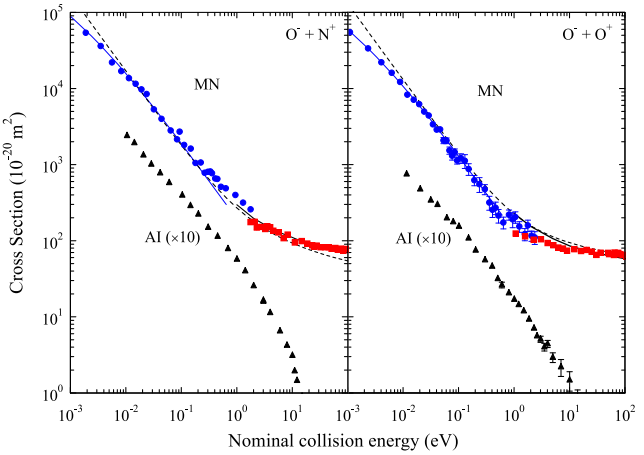

FIG. 2. Total cross sections for $O^- + X^+ \rightarrow O + X^*$ (MN, blue circles from present data; red squares from Ref. [28]) and for $O^- + X^+ \rightarrow XO^+ + e^-$ (AI, black triangles from Ref. [31]) as functions of the nominal collision energy ($\phi = 0$) in Eq. (2). Left panel, $X = N$; right panel, $X = O$. The solid black lines are calculations from Zhou and Dickinson [35] down to 1 eV. The dashed black lines show the present calculations. The blue lines are the convolution of E_{CM}^{-1} cross sections with the angular and energetic distribution of the beams (see text).

$$E_{\mathrm{CM}} = \mu\left(\frac{E_A}{m_A} + \frac{E_B}{m_B} - 2\sqrt{\frac{E_A E_B}{m_A m_B}}\cos\phi\right), \qquad (2)$$

where $\mu = m_A m_B/(m_A + m_B)$ is the reduced mass and ϕ is the angle between the ion trajectories. For 7 keV oxygen beams, $E_A/m_A = E_B/m_B$ and $\phi = 1$ mrad, $E_{\mathrm{CM}} = 3.5$ meV. A typical spread $\Delta E_A \approx 5$ eV in the anion beam energy then gives a negligible spread of $\Delta E_{\mathrm{CM}} \approx 10^{-6}$ eV. The sensitivity to a similar energy spread in the cation beam is equally low. However, a spread in angles $\Delta\phi$ between anion and cation trajectories of 1 mrad, gives $\Delta E_{\mathrm{CM}} \approx 7$ meV.

The ratio between the finite length of the interaction region and the distance to the detectors determines the KER resolution. A longer flight distance gives a better precision on the velocity measurements of the neutrals, and thus it increases the resolution but also limits the angular acceptance. Here, we reach a resolution of 50 meV FWHM at 1 eV of KER, and we are thus able to identify the quantum states (LS terms) of the neutral reaction products.

Total and angular differential MN cross sections can be retrieved from the measured angular distributions. In Fig. 2, we show the present total and absolute MN cross section for $O^- + N^+ \rightarrow O + N^*$ (blue circles, left panel) and for $O^- + O^+ \rightarrow O + O^*$ (blue circles, right panel). The MN absolute cross section scale is established by means of previously measured absolute AI cross sections [31], using the presently measured ratio between AI and MN rates, assuming 50% MCP detection efficiency and correcting for geometrical limitations. This gives a good agreement with the results of Hayton and Peart [28] (red squares) as well as

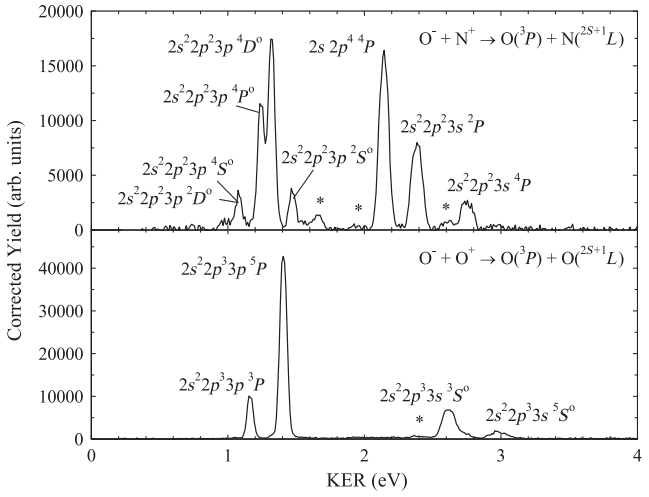

FIG. 3. Kinetic energy release spectra at $E_{CM} = 5$ meV for the MN of $O^- + N^+$ (top panel) and $O^- + O^+$ (bottom panel). The stars indicate contributions from incoming excited cations (see text).

with calculations (solid black line) by Zhou and Dickinson [35] for energies above 1 eV.

The KER distributions for O^- colliding with N^+ (top panel) and with O^+ (bottom panel) are shown in Fig. 3. Each peak in these spectra corresponds to a separate LS term in the excited neutral N (upper panel of Fig. 3) and in the excited O atom (lower panel), while the (other) O atom is found to be in its ground state after it has lost its extra electron. The peaks marked with stars are due to cations in metastable excited states before the interaction. We observe a shift in the peaks' KER of ≈5 meV in relation to their expected positions as given by $\mathrm{KER} = \mathrm{IE}_B - \mathrm{EA}_A - E_B^{\mathrm{exc}}$ with IE_B being the ionization energies of the cations, EA_A the electron affinity of oxygen and E_B^{exc} the $(2J+1)$-weighted mean excitation energy of the statistically populated neutrals formed in electron capture by the cations. Since these spectra were measured at nominal collision energies of 0 eV, according to Eq. (2), with an assumed angle of $\phi = 0$, the shift in energy corresponds to the collision energy E_{CM}, and it is due to the angular spread of the beams.

The area of individual peaks in the KER spectra yields the branching ratios and the corresponding absolute state-selective cross section (by relating the peak area to the total intensity in the KER spectrum). The experimental branching ratios (Expt.) are given in Table I for the $O^- + N^+$ system and shown in Fig. 4 for both systems.

We used the method of Zhou and Dickinson [35], based on a multichannel Landau-Zener (LZ) model and the Firsov-Landau-Herring [36] method, to calculate total and partial cross sections down to 1 meV collision energy for both collision systems. The asymptotic method of Firsov-Landau-Herring allows the evaluation of the one-electron exchange interaction $\Delta(R_X)$, where R_X is the crossing distance, and

TABLE I. Branching ratios (BR in %) for $O^- + N^+ \rightarrow O(^3P) + N(^{2s+1}L)$ at 5 meV CM collision energy for each LS term of N: statistically averaged excitation energy E_{exc} in eV, present experimental results (Expt.), calculations with couplings element from Zhou and Dickinson [35] (ZD) and with MCHF-modified (MCHF) coupling elements (see text).

			BR(%)		
LS term		E_{exc} (eV)	Expt.	ZD	MCHF
$2s^2\ 2p^2\ 3s$	^4P	10.3323	5.11 ± 0.11	0.05	0.04
$2s^2\ 2p^2\ 3s$	^2P	10.6865	16.15 ± 0.18	13.35	8.08
$2s\ 2p^4$	^4P	10.9270	29.99 ± 0.22	1.09	23.17
$2s^2\ 2p^2\ 3p$	$^2S^o$	11.6026	5.34 ± 0.12	4.68	3.58
$2s^2\ 2p^2\ 3p$	$^4D^o$	11.7584	23.25 ± 0.19	50.11	39.69
$2s^2\ 2p^2\ 3p$	$^4P^o$	11.8417	14.74 ± 0.16	22.77	18.82
$2s^2\ 2p^2\ 3p$	$^4S^o$	11.9956	1.44 ± 1.10	1.21	1.02
$2s^2\ 2p^2\ 3p$	$^2D^o$	12.0058	2.79 ± 0.35	6.74	5.60

$H_{if} \sim \Delta(R_X)/2$ is approximately the coupling matrix element between states i and f.

The coupling elements of Zhou and Dickinson (ZD) [35] were first used for the calculation of state-selective cross sections. The corresponding branching ratios were then extracted from the calculated partial cross sections, and they are shown in Table I for collisions with N^+ (at 5 meV) and as functions of the center-of-mass energy in the right panel of Fig. 4 for collisions with O^+. For the latter system, the agreement between experimental and calculated branching ratios at 5 meV for the four states appearing in the KER spectrum is fairly good. However, for the $O^- + N^+$ system, if we compare the calculations (column ZD in Table I) to the experiment, the $2s\ 2p^4\ ^4P$ state is clearly underestimated.

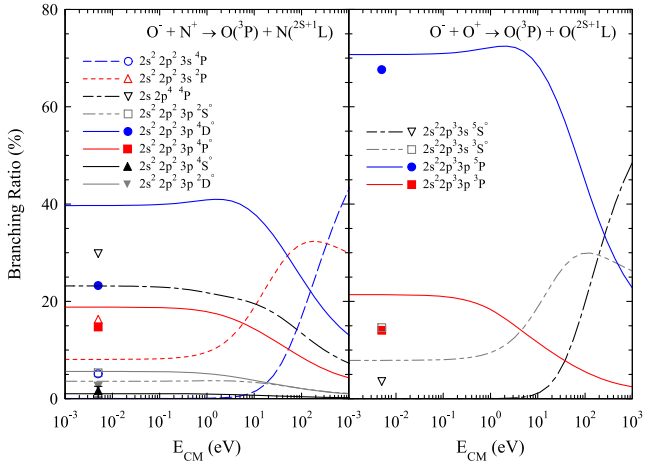

FIG. 4. Branching ratios for $O^- + N^+$ (left) and $O^- + O^+$ (right) as function of E_{CM}. The lines are the present calculations: left panel with MCHF-modified coupling elements and right panel with coupling elements from Ref. [35]. Symbols denote the present experimental results.

In order to investigate the origin of the strong coupling to the $2s\,2p^4\,{}^4P$ state in N, we performed multiconfiguration Hartree-Fock (MCHF) calculations of the $2s\,2p^4\,{}^4P$ energy using an expansion with the three ^4P configurations $2s\,2p^4\,{}^4P$, $2s^2\,2p^2\,3s\,{}^4P$, and $2s^2\,2p^2\,3d\,{}^4P$. This yielded the corresponding mixing coefficients, and these were then used to obtain a modified coupling element for the $\mathrm{N}(2s\,2p^4\,{}^4P)$ state. Branching ratios using coupling strengths based on MCHF calculations are shown in the last column of Table I for 5 meV and in the left panel of Fig. 4, as functions of center-of-mass energy. They are in better agreement with the experiment. However, all of the $2s^2\,2p^2\,3p$ channels, i.e., the channels with low KER, are overestimated by theory, while the $2s\,2p^4\,{}^4P$ and $2s^2\,2p^2\,3s$ channels (high KER) are still underestimated.

Our measurements and calculations clearly show that states, such as $2s\,2p^4\,{}^4P$, populated by a two-electron process cannot be neglected in calculations. Moreover, we can see that multichannel LZ models underestimate high KER channels. In these approaches, only two-by-two couplings at large and intermediate distances are considered, neglecting transitions that may be active at smaller internuclear distances. This was shown by Mitrushchenkov *et al.* [37] for the $\mathrm{Ca}^+ + \mathrm{H}^-$ MN reaction. They compared a branching probability current method with the multichannel approach and showed that the latter underestimates the contribution of weak transitions to the cross section. This effect is important for the $\mathrm{Ca}(3d\,4p\,{}^3F)$ state, which is similar to $\mathrm{N}(2s\,2p^4\,{}^4P)$ since its population implies a two-electron process. However, the branching probability current method can not be applied to $\mathrm{O}^- + \mathrm{N}^+$, as it is too complex for current computational capabilities.

Crossings at short distances are inherently difficult to treat as they are not localized, may overlap with one another, and are affected by the flux branching at the previous crossings along the way to short distances. A way to improve the calculations could be to combine *ab initio* calculations at the smaller distances, with LZ calculations at larger distances. The latter gives enough accuracy for the highly excited electronic states and avoided crossings at large distances, while the former is too complex in that range.

The total cross sections calculated with the coupling elements from Zhou and Dickinson [35] for $\mathrm{O}^- + \mathrm{O}^+$, and from coupling elements modified by means of the present MCHF calculations for $\mathrm{O}^- + \mathrm{N}^+$, are shown by the dashed lines in Fig. 2. They follow the expected E_{CM}^{-1} trend. In both cases, the deviation from the experimental results at low collision energies is a result of the deviation of the actual collision energy from the detuning energy, i.e., the collision energy for perfectly collimated, monoenergetic beams. The convolution of a simulated E_{CM}^{-1} cross section with the angular and energetic distribution of the beams (blue lines) follows the experimental data at low collision energies.

In conclusion, we have presented the first measurements of absolute *state-selective* mutual neutralization cross sections *at subthermal energies*. This has been demonstrated for $\mathrm{O}^- + \mathrm{N}^+$ and $\mathrm{O}^- + \mathrm{O}^+$ collisions at energies ranging from 5 meV to 2 eV. The measured total mutual neutralization cross sections above 1 eV are in very good agreement with previous measurements from Hayton and Peart [28]. We calculated the cross sections and branching ratios down to 1 meV using the method by Zhou and Dickinson [35] to arrive at coupling strengths, which were then used in multichannel LZ calculations. Using this procedure, we reached a reasonable agreement for $\mathrm{O}^+ + \mathrm{O}^-$, but in the case of $\mathrm{N}^+ + \mathrm{O}^-$, the population of the channel labeled $2s\,2p^4\,{}^4P$ could only be accounted for if the strong configuration interaction in this LS term was considered. We expect that results at subthermal energies of the present quality will be crucial for modeling the charge balance and ion excitation energies in cold astrophysical environments. They can also contribute to a better understanding of the ultraviolet ionospheric nightglow at 135.6 nm, as we observe a dominant population of $\mathrm{O}(^5P)$ supporting the two-step model via $\mathrm{O}(^5P) \rightarrow \mathrm{O}(^5S) \rightarrow \mathrm{O}(^3P)$.

In the present experiment, we could see small contributions from metastable excited states in the incoming ion beams. Such effects will almost always be a problem in merged beams experiments with *molecular* ions. At the DESIREE (double electrostatic storage ring experiment) infrastructure at Stockholm University [38,39], beams of anions and cations can be stored for long times, relax to the lowest quantum states [40], and can be merged for studies of mutual neutralization at very low temperatures and well defined collision energies. Our present studies with atomic reactants will serve to benchmark similar experiments conducted with DESIREE.

The authors thank M. Godefroid and J. Loreau for advice concerning the MCHF and Landau-Zener calculations and Å. Larson for stimulating discussions. This work was supported by the Fonds de la Recherche Scientifique–FNRS (IISN Contract No. 4.4504.10) and by the Swedish Research Council (Contracts No. 2017-00621, No. 621-2014-4501, and No. 621-2015-04990). T. L. is funded by a fellowship of the Fonds pour la Formation à la Recherche dans l'Industrie et dans l'Agriculture-FRIA.

[1] D. Smith and P. Spanel, Mass Spectrom. Rev. **14**, 255 (1995).
[2] A. Chutjian, A. Garscadden, and J. Wadehra, Phys. Rep. **264**, 393 (1996).
[3] M. Larsson, W. D. Geppert, and G. Nyman, Rep. Prog. Phys. **75**, 066901 (2012).
[4] V. Vuitton, P. Lavvas, R. V. Yelle, M. Galand, A. Wellbrock, G. R. Lewis, A. J. Coates, and J. E. Wahlund, Planet. Space Sci. **57**, 1558 (2009).
[5] R. Wildt, Astrophys. J. **89**, 295 (1939).
[6] L. M. Branscomb and B. E. J. Pagel, Mon. Not. R. Astron. Soc. **118**, 258 (1958).

[7] M. S. Vardya, Mem. R. Astron. Soc. **71**, 249 (1967).
[8] A. Dalgarno and R. A. McCray, Astrophys. J. **181**, 95 (1973).
[9] E. Herbst, Nature (London) **289**, 656 (1981).
[10] M. C. McCarthy, C. A. Gottlieb, H. Gupta, and P. Thaddeus, Astrophys. J. **652**, L141 (2006).
[11] J. Cernicharo, M. Guélin, M. Agundez, K. Kawaguchi, M. McCarthy, and P. Thaddeus, Astron. Astrophys. **467**, L37 (2007).
[12] S. Brünken, H. Gupta, C. A. Gottlieb, M. McCarthy, and P. Thaddeus, Astrophys. J. **664**, L43 (2007).
[13] P. Thaddeus, C. A. Gottlieb, H. Gupta, S. Brünken, M. C. McCarthy, M. Agúndez, M. Guélin, and J. Cernicharo, Astrophys. J. **677**, 1132 (2008).
[14] J. Cernicharo, M. Guélin, M. Agundez, M. McCarthy, and P. Thaddeus, Astrophys. J. Lett. **688**, L83 (2008).
[15] M. Agundez, J. Cernicharo, M. Guélin, C. Kahane, E. Roueff, J. Klos, F. J. Aoiz, F. Lique, N. Marcelino, J. R. Goicoechea *et al.*, Astron. Astrophys. **517**, L2 (2010).
[16] N. Harada and E. Herbst, Astrophys. J. **685**, 272 (2008).
[17] D. R. Flower, G. Pineau Des Forêts, and C. M. Walmsley, Astron. Astrophys. **474**, 923 (2007).
[18] M. A. Cordiner and S. B. Charnley, Astrophys. J. **749**, 120 (2012).
[19] T. Millar, C. Walsh, M. Cordiner, R. Ní Chuimín, and E. Herbst, Astrophys. J. **662**, L87 (2007).
[20] V. Wakelam and E. Herbst, Astrophys. J. **680**, 371 (2008).
[21] C. Walsh, N. Harada, E. Herbst, and T. J. Millar, Astrophys. J. **700**, 752 (2009).
[22] V. Wakelam, E. Herbst, J.-C. Loison, I. W. M. Smith, V. Chandrasekaran, B. Pavone, N. G. Adams, M.-C. Bacchus-Montabonel, A. Bergeat, K. Béroff, V. M. Bierbaum *et al.*, Astrophys. J. Suppl. Ser. **199**, 21 (2012).
[23] D. McElroy, C. Walsh, A. J. Markwick, M. A. Cordiner, K. Smith, and T. J. Millar, Astron. Astrophys. **550**, A36 (2013).
[24] M. A. Cordiner and S. B. Charnley, Meteorit. Planet. Sci. **49**, 21 (2014).
[25] J. Qin, J. J. Makela, F. Kamalabadi, and R. R. Meier, J. Geophys. Res.: Space Phys. **120**, 10116 (2015).
[26] E. Sagawa, T. J. Immel, H. U. Frey, and S. B. Mende, J. Geophys. Res.: Space Phys. **110**, A11302 (2005).
[27] R. E. Olson, J. R. Peterson, and J. Moseley, J. Geophys. Res. **76**, 2516 (1971).
[28] D. A. Hayton and B. Peart, J. Phys. B **26**, 2879 (1993).
[29] M. Terao, S. Szücs, M. Cherkani, F. Brouillard, R. J. Allan, C. Harel, and A. Salin, Europhys. Lett. **1**, 123 (1986).
[30] S. M. Nkambule, N. Elander, A. Larson, J. Lecointre, and X. Urbain, Phys. Rev. A **93**, 032701 (2016).
[31] T. Nzeyimana, E. A. Naji, X. Urbain, and A. Le Padellec, Eur. Phys. J. D **19**, 315 (2002).
[32] B. Fabre, Ph.D. thesis, Université catholique de Louvain, 2005, https://dial.uclouvain.be/pr/boreal/object/boreal:5372.
[33] S. Szücs, M. Karemera, M. Terao, and F. Brouillard, J. Phys. B **17**, 1613 (1984).
[34] F. Brouillard and W. Claeys, in *Physics of Ion-Ion and Electron-Ion Collisions*, edited by F. Brouillard and W. Claeys (Plenum Press, New York, 1983) pp. 415–459.
[35] X. Zhou and A. Dickinson, Nucl. Instrum. Methods B **124**, 5 (1997).
[36] M. Chibisov and R. Janev, Phys. Rep. **166**, 1 (1988).
[37] A. Mitrushchenkov, M. Guitou, A. K. Belyaev, S. A. Yakovleva, A. Spielfiedel, and N. Feautrier, J. Chem. Phys. **146**, 014304 (2017).
[38] R. D. Thomas, H. T. Schmidt, G. Andler, M. Björkhage, M. Blom, L. Brännholm, E. Bäckström, H. Danared, S. Das, N. Haag *et al.*, Rev. Sci. Instrum. **82**, 065112 (2011).
[39] H. T. Schmidt, R. D. Thomas, M. Gatchell, S. Rosén, P. Reinhed, P. Löfgren, L. Brännholm, M. Blom, M. Björkhage, E. Bäckström *et al.*, Rev. Sci. Instrum. **84**, 055115 (2013).
[40] H. T. Schmidt, G. Eklund, K. C. Chartkunchand, E. K. Anderson, M. Kamińska, N. de Ruette, R. D. Thomas, M. K. Kristiansson, M. Gatchell, P. Reinhed, S. Rosén, A. Simonsson, A. Källberg, P. Löfgren, S. Mannervik, H. Zettergren, and H. Cederquist, Phys. Rev. Lett. **119**, 073001 (2017).